CAT & MAUS: a novel system for true dynamic motion measurement of underlying bony structures with compensation for soft tissue movement

Rui Jia, Paul Monk, David Murray, J. Alison Noble, Stephen Mellon

PII: S0021-9290(17)30214-2
DOI: http://dx.doi.org/10.1016/j.jbiomech.2017.04.015
Reference: BM 8196

To appear in: *Journal of Biomechanics*

Accepted Date: 9 April 2017

Please cite this article as: R. Jia, P. Monk, D. Murray, J. Alison Noble, S. Mellon, CAT & MAUS: a novel system for true dynamic motion measurement of underlying bony structures with compensation for soft tissue movement, *Journal of Biomechanics* (2017), doi: http://dx.doi.org/10.1016/j.jbiomech.2017.04.015

CAT & MAUS: a novel system for true dynamic motion measurement of underlying bony structures with compensation for soft tissue movement

Rui Jia[a,*], Paul Monk[b], David Murray[b], J.Alison Noble[a], Stephen Mellon[b]

[a] *Institute of Biomedical Engineering, Department of Engineering Science, University of Oxford, Oxford, UK*
[b] *Oxford Orthopaedic Engineering Centre, Nuffield Department of Orthopaedics, Rheumatology and Musculoskeletal Sciences, University of Oxford, Oxford, UK*

Abstract

Optoelectronic motion capture systems are widely employed to measure the movement of human joints. However, there can be a significant discrepancy between the data obtained by a motion capture system (MCS) and the actual movement of underlying bony structures, which is attributed to soft tissue artefact. In this paper, a computer-aided tracking and motion analysis with ultrasound (CAT & MAUS) system with an augmented globally optimal registration algorithm is presented to dynamically track the underlying bony structure during movement. The augmented registration part of CAT & MAUS was validated with a high system accuracy of 80 %. The Euclidean distance between the marker-based bony landmark and the bony landmark tracked by CAT & MAUS was calculated to quantify the measurement error of an MCS caused by soft tissue artefact during movement. The average Euclidean distance between the target bony landmark measured by each of the CAT & MAUS system and the MCS alone varied from 8.32 mm to 16.87 mm in gait. This indicates the discrepancy between the MCS measured bony landmark and the actual underlying bony landmark. Moreover, Procrustes analysis was applied to demonstrate that CAT & MAUS reduces the deformation of the body segment shape modelled

*Corresponding author
Email address: rui.jia@eng.ox.ac.uk (Rui Jia)

by markers during motion. The augmented CAT & MAUS system shows its potential to dynamically detect and locate actual underlying bony landmarks, which reduces the MCS measurement error caused by soft tissue artefact during movement.

Keywords: Computer-aided tracking, motion analysis, ultrasound, soft tissue artefact, hip joint, gait

1. Introduction

Optoelectronic motion capture systems (MCS), for example VICON systems (*Oxford, UK*), are commonly employed to monitor and measure motions of the human body. An optoelectronic MCS is composed of a group of infra-red cameras that capture the trajectories of skin-attached retro-reflective markers to determine the movement of corresponding underlying bony landmarks. However, because of soft tissues between the skin and the underlying bone, for example muscles and fat, sliding, stretching and compressing during movement, the skin-attached markers shift away from the original bony landmarks [20]. This leads to a significant discrepancy between the data obtained by an MCS and the actual movement of underlying bone structures and this is attributed to soft tissue artefact (STA). It has been reported that STA can cause an MCS measurement error of up to 30 mm for the thigh [1][17][20].

In order to correct the error caused by soft tissue movement, it is essential to first track and assess the movement of actual underlying bony structures. This can be done by either tracking the bone by attaching invasive pins to the underlying bone landmarks [15] or by imaging the actual bone during movement. Several medical imaging technologies, such as open magnetic resonance imaging (MRI) [4][19] and X-ray radiography [18][20], have been employed to image the underlying bony structures and track their motion for comparison to the MCS data in order to quantify the effects of STA. However, these imaging studies have suffered from, for example, the limited field of view of devices or the excessive exposure to radiation which may increase the risk of cancer to

the subject[12]. Compared to MRI and X-ray imaging, ultrasound (US) is a cheaper, more dynamic, more portable and non-ionising imaging modality [14]. It has shown some potential for tracking underlying bony structures instead of skin-attached markers [3][13]. However, imaging large joints such as the hip and the knee presents its own challenge due to the limited footprint of most US transducers. Moreover, in previous US-related methods, the target structures had to be identified by eye, making US-based measurement laborious and time consuming [13]. The potential of using ultrasound imaging to very accurately explore human joint motion has also been explored by Masum *et al.,* [10][11] with a novel multi-probe approach.

A computer-aided tracking and motion analysis with ultrasound (CAT & MAUS) system has been developed by our group to track the underlying bony anatomy in 3D space during routine activities, for example gait. It combines state-of-the-art computer vision techniques, including an automatic US segmentation, a 3D reconstruction and a 3D surface-to-surface registration, with an MCS and a 2D US device. In a previously published paper [9], our CAT & MAUS system was applied to estimate hip joint kinematics during gait. The difference between the actual position of the underlying bony structure and the position captured by marker-based MCS alone during gait was illustrated using CAT & MAUS. However, the 3D bone surfaces for the surface-to-surface registration were reconstructed from 2D US sweeps at static gait poses. Since gait is a continuous sequence, the nature of the examination did not capture the continuity and reality of dynamic gait. This approach is not capable of dynamically measuring hip joint kinematics. The 3D position of the femur surface can be reconstructed for motion data using the skin markers but STA affects the accuracy. Data recorded by the US probe about the bone position during motion can be used to adjust the 3D position of the reconstructed femur surface and in the process compensate for STA.

In this paper, we have augmented our previous CAT & MAUS system with a multiple segments globally optimal registration algorithm to dynamically locate a target bony landmark. The ability of this system to dynamically locate the

greater trochanter (GT) in 3D space during gait was explored. In addition the potential for the system to compensate for STA during gait was investigated.

2. Methods

2.1. Computer-aided tracking and motion analysis with ultrasound

A computer-aided tracking and motion analysis with ultrasound (CAT & MAUS) system combines a computer-aided post-processing pipeline with a motion analysis with ultrasound (MAUS) system [13]. A schematic of the CAT & MAUS system is shown in Fig. 1.

The constitution of the MAUS part of the CAT & MAUS system shares similar principles with three-dimensional (3D) freehand US imaging [7]. Thus, it is comprised of an optoelectronic MCS (*VICON, Oxford, UK*) and a 2D US system (*LOGIQ S7, GE, USA*). Four 10 mm diameter retro-reflective markers were attached in a cruciform layout to a bespoke 3D printed thermoplastic case that covers a *ML 6-15* US transducer. These markers provide location information for the US transducer. The MAUS system is spatially and temporally calibrated before experiments. The acquired MCS data and US data are then processed in Matlab R2014a (*Mathworks, USA*) on a desktop computer (*8-core Intel Core i7-4770 3.40 GHz running a 64-bit Windows OS*) for computer-aided post-processing.

The computer-aided tracking pipeline is composed of an automatic bone segmentation (Fig. 1b) [6] and a globally optimal 3D surface-to-surface registration (Fig. 1c) [8] followed by a quantification analysis of hip joint kinematics according to an adapted definition of hip joint kinematics from the International Society of Biomechanics [9] (Fig. 1d). Firstly, the bone structures in US images are automatically segmented as a precursor to reconstruct 3D bone surfaces at different body poses. Then, the transformation between two 3D surfaces reconstructed at two different poses is obtained from the registration procedure to locate the target bony structure from one pose to another. For a detailed description of the automatic image analysis methods, refer to [6][7][8][9].

2.2. Multiple segments globally optimal registration

In [8], surface patches of a bone-of-interest, i.e. a GT, were scanned and reconstructed by CAT & MAUS at static gait poses and registered to the reference surface at the standing pose to calculate the transformation between surfaces at different poses so that the position of the bone-of-interest could be determined. Since the static poses were only a representation of instances from gait, it is likely that this method underestimates the effect of STA. To tackle this issue, a multiple segments globally optimal registration algorithm is applied to data retrieved from the US transducer while subjects carried out dynamic gait on a treadmill.

Since only one US frame can be captured at a single gait event during the dynamic measurement, the transformed bone contour of a given frame in 3D space is registered to the 3D reference surface reconstructed at the upright standing pose using the globally optimal registration algorithm [8]. The registration algorithm results in an optimal solution by a 3D global branch-and-bound search to minimise the L_2 norm. The convergence threshold of the optimization is set empirically [8]. However, when this bone contour with relatively limited geometry information is registered to a 3D reference surface with much more points but little morphological diversity, i.e. the surface shape is quite uniform, the registration may fail as the algorithm finds more than one solution that satisfies the threshold of the L_2 norm. There is then no reliable way to tell which one is the correct solution. A correct solution could be obtained after many more iterations to further minimise the L_2 norm with respect to an even smaller threshold (for example zero) but this was extremely time consuming (approx. 6 hours) and was ruled out. Instead a multiple segments approach was developed in an attempt to register the bone contour to the 3D reference surface more accurately.

To conduct the multiple segments globally optimal registration, the 3D reference surface is evenly divided into n segments from proximal to distal. This reduces the difference in the number of points between the bone contour and the reference segment. In this study, the full reference surface is split into 3

segments (Fig. 2). During data acquisition the scanning angle of the transducer is adjusted to track the same target bony structure during dynamic measurement, it is unlikely that the transducer is moved along the object bone by more than one third of the scanned area (approximately 10 mm) nor tilted by more than 30° (approximately 3 mm). In practice, the boundaries at the junctions between the three segments were extended and overlapped by 3 mm to avoid the case that the optimal solution crosses the junctions. Two segments did not reduce the execution time significantly while three segments were the minimum required to reduce the execution time without the need to reduce the threshold.

Next, the segmented bony structure of a given US frame during movement is registered to each of the reference segments using the globally optimal registration. The best solution i.e. the one with the minimal L_2 norm, is then selected out of the three solutions. Finally, the target bony landmark is located by using the transformation returned by the registration. An illustration of the multiple segments globally optimal registration is shown in Fig. 2.

2.3. Procrustes analysis

In this study, the femur shape was made up from a finite number k ($k = 5$) of landmarks in 3D space, which were the greater trochanter, the lateral femoral epicondyle, the medical femoral epicondyle, the anterior mid thigh and the lateral mid thigh (wand marker) [5]. To illustrate that CAT & MAUS reduces the deformation of the femur shape caused by STA relative to MCS alone, Procrustes analysis [16] was applied to compare the left femur shape made up with each of the MCS GT and the CAT & MAUS GT separately at an example gait pose to the corresponding femur shape at the standing pose while the other four markers were unchanged. The same gait poses in both CAT & MAUS data and MCS data were manually found from the MCS software (*Nexus 2.2.2, VICON, Oxford, UK*). The femur shape at the standing pose in 3D space is denoted as:

$$((x_1, y_1, z_1), (x_2, y_2, z_2), ..., (x_i, y_i, z_i), ..., (x_k, y_k, z_k))$$

and the femur shape at an example gait pose is denoted as:

$$((u_1, v_1, w_1), (u_2, v_2, w_2), ..., (u_i, v_i, w_i), ..., (u_k, v_k, w_k)).$$

Before shape comparison, two shapes are superimposed by translation, rotation and uniform scaling.

All the bony landmarks of the shape are translated to the centroid by subtracting the mean of all the landmarks that make up the femur shape, which means the i^{th} landmark (x_i, y_i, z_i) is translated to $(x_i - \overline{x}, y_i - \overline{y}, z_i - \overline{z})$, where $\overline{x} = \frac{x_1+x_2+...+x_i+...+x_k}{k}$, $\overline{y} = \frac{y_1+y_2+...+y_i+...+y_k}{k}$ and $\overline{z} = \frac{z_1+z_2+...+z_i+...+z_k}{k}$. Similar to the translation, the scaling factor of the femur shape is made uniform by dividing by the root mean square $s = \sqrt{\frac{\sum_{i=1}^{k}(x_i-\overline{x})^2+(y_i-\overline{y})^2+(z_i-\overline{z})^2}{k}}$, i.e. the i^{th} landmark (x_i, y_i, z_i) was scaled to $(\frac{x_i-\overline{x}}{s}, \frac{y_i-\overline{y}}{s}, \frac{z_i-\overline{z}}{s})$. For rotation, the shape

$$((x_1, y_1, z_1), (x_2, y_2, z_2), ..., (x_i, y_i, z_i), ..., (x_k, y_k, z_k))$$

is set as the reference orientation. The shape

$$((u_1, v_1, w_1), (u_2, v_2, w_2), ..., (u_i, v_i, w_i), ..., (u_k, v_k, w_k))$$

is then rotated around the origin. The angles of rotation α, β and γ around the x, y and z axes respectively are optimized by minimising the sum of the squared distances between the corresponding landmarks. The two shapes are translated, scaled and rotated for shape comparison. The superimposed two shapes are denoted as

$$((X_1, Y_1, Z_1), (X_2, Y_2, Z_2), ..., (X_i, Y_i, Z_i), ..., (X_k, Y_k, Z_k))$$

and

$$((U_1, V_1, W_1), (U_2, V_2, W_2), ..., (U_i, V_i, W_i), ..., (U_k, V_k, W_k))$$

respectively.

After superimposing the two shapes, the difference in the femur shape is evaluated by calculating the Procrustes distance (PD), which is defined as the

square root of the sum of the squared distances between corresponding normalised landmark locations as in Equation 1.

$$PD = \sqrt{\sum_{i=1}^{k} (U_i - X_i)^2 + (V_i - Y_i)^2 + (W_i - Z_i)^2} \quad (1)$$

A PD of zero indicates the shapes are identical.

Moreover, the Euclidean distance between the GT of each of these two superimposed femur shapes was also calculated to quantify the mismatch of the measured bony landmark caused by STA.

3. Experiments

3.1. In-vitro validation of multiple segments globally optimal registration

To validate the accuracy of the augmented registration algorithm, a proximal femur phantom with a socket ball joint was used. Four 10 mm diameter retro-reflective markers were attached to four non-coplanar positions of the femur shaft to provide femur location information as the ground truth as illustrated in Fig. 3a. Another four markers were attached at each corner of the water tank to provide position information of the water tank (Fig. 3b). If the calibration box was moved during the experiment, these four markers could be used to correct the displacement. The water tank had a Mylar sheet window in the front wall through which the femur phantom was scanned. The femur phantom was then clamped in the water tank and could be rotated in three degrees of freedom (3DOF), as shown in Fig. 3b.

The water tank was filled with degassed water to submerge the target bony landmark (i.e. the GT) so that it could be captured by ultrasound. The retro-reflective markers attached to the femur phantom were remained above the water line as the markers cannot be tracked in water. Firstly, the GT at a static position was scanned in a tracked sweep of the US transducer and reconstructed as the reference surface. Then the femur phantom, which had 3DOF, was rotated arbitrarily. The position of the US transducer was adjusted to make sure the GT was imaged within the transducer's field of view throughout

the femur phantom rotation. The sampling frequency of the 2D US transducer was set to 23 Hz (45 mm US depth) while the sampling frequency of the MCS was 100 Hz. Since the femur phantom was arbitrarily rotated for around 10 seconds in three trials, over 600 US frames were captured. Twenty US frames were randomly selected to determine the accuracy of the multiple segments registration approach. The bone structures in these 20 frames were automatically segmented [6] and registered to each of three split reference segments to obtain the optimal solution. Finally, the registration result was compared to the result of full reference surface registration and the ground truth from MCS markers on the femur phantom.

3.2. In-vivo experiment

Ten healthy volunteers (5 males and 5 females) with a mean age of 26 years ranging from 18 to 36 were recruited. Anthropometric parameters were measured including the height, weight, left leg length and foot length. All the volunteers were slim to average body-build (weights: 49.4 kg - 68.1 kg; heights: 160.1 cm - 185.2 cm). The average body mass index (BMI) was 20.2 ranging from 18.9 to 21.7. The experiment was conducted on each volunteer's left leg. The average left leg length of the females was 91.2 cm and 99.3 cm for males. All ten volunteers had no known hip joint conditions and no joint replacements.

Twenty eight lower limb bony landmarks of each subject were represented by twenty eight 10 mm diameter retro-reflective markers by following a standard Helen Hayes configuration [2] with another ten extra markers on the lower limbs. Refer to [9] for a detailed description of marker attachment. Each volunteer was then examined three times using each of the MCS alone and the CAT & MAUS system.

A volunteer was firstly asked to perform the upright standing pose and the gait at 3 mph on a treadmill with the full set of markers. Marker trajectories were captured by the MCS. Then, the marker on the left GT of the volunteer was removed. Instead of a skin-attached marker, the left GT was scanned by an US sweep to reconstruct a 3D reference surface at the standing pose (red surface in

Fig. 2). A detailed description of the US scanning protocol and 3D bone surface reconstruction can be found in [7][9]. After that, the volunteer was asked to walk again at 3 mph on the treadmill while the 2D US transducer was hand-held by an operator to image the left GT during gait. The transducer position was adjusted to keep the bone surface within the US field of view throughout the gait cycle. Meanwhile, the position of the transducer was captured by the MCS. Since the bone may be missed during dynamic US imaging because of the limited field of view, the volunteer was asked to perform more than ten gait cycles to guarantee the bone was captured at all gait events. By following the augmented computer-aided tracking pipeline, the bone contours were automatically segmented and registered to the 3D reference surface during gait. Procrustes analysis was then applied to analyze the deformation of both the MCS left femur shape and the CAT & MAUS femur shape at four different poses (heel strike, mid stance, toe off and mid swing as in Fig. 4) compared to the MCS reference femur shape and the CAT & MAUS reference femur shape at the standing pose respectively.

Finally, the Euclidean distance between the CAT & MAUS GT and the MCS GT of the superimposed MCS and CAT & MAUS femur shapes at the same pose was calculated to quantify the estimated error caused by STA.

4. Results and Discussion

4.1. In-vitro validation

A visual comparison of the registration results from the segmented bone contour in a given US frame captured by US during movement to the full reference surface and to each of three split segments are shown in Fig. 5. The blue line is the segmented bone contour of one example US frame, while the red point cloud is the reference surface. Although the results of registration to the full reference surface (Fig. 5b), Segment 2 or Segment 3 (Fig. 5c) are all within the threshold of the L_2 norm, it can be seen that the bone contour in 3D space was better aligned with Segment 1 than the others (Fig. 5c), which gave the best registration result. The normalised L_2 norms of registrations to the full

reference surface and each of those three segments, and the reference with the minimum L_2 norm are listed in Table 1a. It can be seen that the registration to multiple segments gave a smaller L_2 norm than the registration to the full reference surface.

To further assess the accuracy of the results from the registration, the rotations derived from transformation matrix were compared to the rotation ground truth provided by the four non-coplanar markers on the femur phantom. The mean rotation angle difference between the ground truth and results from the registrations to the full reference surface and each of those three segments, and the reference with the minimum absolute value of the mean rotation angle difference are listed in Table 1b. It is shown that the registration to the full reference surface can cause a rotation error of up to 32.27° which exceeds the clinical tolerance (±5°) [12]. This indicates that the previous global optimal registration may fail when the data contains insufficient morphological information. Ideally, if the multiple segments registration is 100 % accurate, this mean rotation angle difference of the Segment with the optimal solution should be zero degrees and its reference index should match the optimal reference index listed in the last column of Table 1a. The optimal reference index of the optimal registration result that had the smallest absolute value of mean difference in rotation angle to the ground truth (Table 1b) was often found to be the reference index with the minimum L_2 norm (Table 1a). There were only four out of twenty positions where the optimal reference index of the registration with smallest absolute value of mean difference in rotation angle did not match the optimal reference index of the registration with the minimum L_2 norm (highlighted in a gray color), which gives a system accuracy of 80%. Herein, we define the system accuracy as the successful match instances (16) as a percentage of the total registrations carried out (20).

Moreover, a segmented bone contour with unique morphological signatures, such as a notch (Fig. 6a), was registered to the reference more accurately than a plain bone structure (Fig. 6b). The bone structure with a notch was captured at position 12 and 16 in Table 1a and 1b, which resulted in smaller L_2 norms

and rotation angle difference. This is due to the unique morphological signature (the notch) which helps the registration to match to the same signature of the reference surface.

The elapsed time for a single full surface registration with a stop threshold of 0.01 varied from 10 to 45 minutes depending on the shape of the 2D bone structure and the number of reference surface points, while one multiple segments registration globally optimal registration with a stop threshold of 0.01 only took approximately 3-5 minutes. Although the full surface registration took more time, it may still fail when the 2D bone structure has less morphological information. This is because more possibilities satisfy the threshold during the optimization procedure.

4.2. In-vivo experiment

The mean Procrustes distances between the CAT & MAUS femur shape at four different gait poses (heel strike, mid stance, toe off and mid swing) and the CAT & MAUS reference femur shape at the standing pose were 0.05 ± 0.03, 0.02 ± 0.01, 0.02 ± 0.01 and 0.03 ± 0.01 respectively, which are listed in Table 2a. The mean Procrustes distances for MCS alone were 0.20 ± 0.05, 0.16 ± 0.06, 0.16 ± 0.05 and 0.23 ± 0.05 relative to those four gait poses and are listed in Table 2b.

Comparing Table 2a with Table 2b, the Procrustes distances between the CAT & MAUS femur shape at four gait poses and CAT & MAUS reference femur shape at the standing pose are smaller than the Procrustes distances between the MCS femur shape at four gait poses and MCS reference femur shape at the standing pose. This indicates that the femur shape reconstructed by the MCS alone deforms more that the femur shape reconstructed by CAT & MAUS during gait. This is because that the GT marker captured by the MCS alone shifted away from the actual underlying GT due to STA. CAT & MAUS reduces the marker-based measurement error of the bony landmarks as the CAT & MAUS GT avoid suffering from STA. Fig. 7a illustrates the difference between the femur shapes captured at the standing pose by the MCS alone and CAT &

MAUS. The femur shapes captured by the MCS alone and CAT & MAUS at one example gait pose of those four gait poses are compared in Fig. 7b. To explain the shape deformation during movement caused by STA, the femurs modelled by each of the MCS alone and CAT & MAUS at the standing pose and one example gait pose of those four gait poses were compared in Fig. 7c. In this study, it was assumed that the other skin-based markers performed the same at any given gait pose due to the repeatability of gait. As the CAT & MAUS system detected the actual underlying GT, the GT detected at the standing pose and the other gait poses was expected to be the same bony landmark (the black and blue coincident point in Fig. 7c). Moreover, as only the GT was captured using both techniques (MCS alone and CAT & MAUS), the other four markers attached on the femur were assumed to be in the same positions during the examinations using MCS alone and CAT & MAUS at each gait pose (the yellow and black coincident points at the standing pose in Fig. 7a and 7c, and the red and blue coincident points at one gait pose in Fig. 7b and 7c. Since all five markers shifted away because of STA in MCS alone, while only four markers changed (exclude GT) in CAT & MAUS measurement, from Fig. 7c, it can be seen that the red segment compared to the original yellow segment deforms more than the blue segment compared to the original black segment. Thus, the CAT & MAUS Procrustes distances are smaller than the MCS Procrustes distances (Table 2).

The Euclidean distances between the CAT & MAUS GT and the MCS GT of the superimposed MCS and CAT & MAUS femur shapes at the same pose are shown in Fig. 8. The average Euclidean distance over the ten subjects was $14.57 \pm 5.51mm$, $8.32 \pm 3.11mm$, $13.27 \pm 1.85mm$ and $16.87 \pm 7.74mm$ at heel strike, mid stance, toe off and mid swing respectively, while the average Euclidean distance over the ten subjects was $8.86 \pm 1.43mm$ at the standing pose. Moreover, the smallest difference of the average Euclidean distance to the standing pose was at the mid stance pose ($1.54 \pm 1.68mm$). This is because the reference leg at a mid stance pose is similar to the reference leg at the standing pose. The Euclidean distance indicates the offset between the marker-based

GT and the actual underlying GT detected by CAT & MAUS. This distance is highly related to the soft tissue content, i.e. how much soft tissue between the bone surface and the skin surface. Since soft tissue content varies from person to person, a person with high soft tissue content may suffer from the severe STA which may result in a bigger marker-based measurement error (i.e. a bigger Euclidean distance). Since all the subjects in this study were slim, the average Euclidean distance varied from 8.32 mm to 16.87 mm which was smaller than the reported error of up to 30 mm for the thigh caused by STA [1][17][20]. However, this is not the only reason. An imprecise marker attachment to a given bony landmark may also introduce a large Euclidean distance error.

The Procrustes analysis results shows the potential of the CAT & MAUS system to reduce femur shape deformation during movement caused by STA. The Euclidean distance estimates the displacement of the marker shifted away from the actual bony landmark, which can be used to compensate the MCS measurement error due to STA. However, the system accuracy of this augmented CAT & MAUS is dependent on the morphological signatures of the segmented bone structure. Erroneous extraction of the target bony structure using CAT & MAUS has to be manually corrected which is a limitation as observer error then becomes an issue. Thus, a suitable scanning protocol suggested by US radiographers for capturing more morphological signatures reliably could be a solution for increasing the system accuracy and potentially making the system more suitable for clinical use.

Other limitations include the fact that CAT & MAUS is currently only optimised to detect and measure the position of the femur surface in the region of the greater trochanter. This means the system can only currently compensate for STA occurring for one marker. Describing the kinematics of the femur is still reliant on the other skin mounted markers and so STA cannot be eliminated. Use of a probe array or a probe at another location of the femur could address these problems. Masum et al., [10] have made some progress in validating the accuracy of a tri-plane US system for measuring kinematics. However the current discrepancy in sampling rate between US systems (23 Hz) and motion

analysis systems (100 Hz) currently limits the amount of information that can be processed on, for example, a typical gait cycle that lasts approximately one second.

5. Conclusions

In this paper, an augmented computer-aided tracking and motion analysis with ultrasound (CAT & MAUS) system has been introduced to dynamically measure the movement of the GT during gait. A multiple segments globally optimal registration has been developed to dynamically locate the underlying bony structure during movement. It has been validated with a proximal femur phantom shown that the multiple segments registration algorithm is more accurate than the full surface registration with a high system accuracy of 80%. The *in-vivo* CAT & MAUS results have been compared to the results captured by a commercial motion capture system (MCS). From Procrustes analysis of the results from both systems, it has been shown that CAT & MAUS reduces the deformation of marker-modelled shape during movement. As the CAT & MAUS system describes the movement of actual underlying bony landmarks, it significantly reduces the measurement error of an MCS due to STA and it is well-suited as a measurement tool for clinical research of joint kinematics. With the increasing availability of wireless US probes in conjunction with future US array miniaturisation suggests it is likely that a combination of motion analysis and US imaging will eventually become one of the most accurate methods for experimentally determining bone pose during motion.

Acknowledgements

The authors would like to thank Orthopaedics Research UK for supporting this project (Grant code: HFR00390) and the China Scholarship Council for funding Rui Jia (CSC NO.201408060234). We sincerely thank all the participants for volunteering in the experiments.

Conflict of interest

The authors declare that they have no conflict of interest.

Ethical standard

All the *in-vivo* experiments were in accordance with the ethical standards of the institutional and/or national research committee.

References

[1] Akbarshahi, M., Schache, A.G., Fernandez, J.W., Baker, R., Banks, S., Pandy, M.G., 2010. Non-invasive assessment of soft-tissue artifact and its effect on knee joint kinematics during functional activity. Journal of Biomechanics 43, 1292–1301.

[2] Collins, T.D., Ghoussayni, S.N., Ewins, D.J., Kent, J.A., 2009. A six degrees-of-freedom marker set for gait analysis: repeatability and comparison with a modified helen hayes set. Gait & Posture 30, 173–180.

[3] Herrington, L., McEwan, I., Thom, J., 2006. Quantification of patella position by ultrasound scanning and its criterion validity. Ultrasound in Medicine & Biology 32, 1833–1836.

[4] Higuchi, T., Arai, Y., Takamiya, H., Miyamoto, T., Tokunaga, D., Kubo, T., 2010. An analysis of the medial patellofemoral ligament length change pattern using open-mri. Knee Surgery, Sports Traumatology, Arthroscopy 18, 1470–1475.

[5] Jia, R., Hansjee, S., Monk, A.P., Murray, D., Noble, J.A., Mellon, S., 2016a. Cat & maus: Elucidation of hip joint kinematics in gait and comparison with motion analysis, in: IET Human Motion Analysis for Healthcare Applications, BMVA.

[6] Jia, R., Mellon, S., Hansjee, S., Monk, A.P., Murray, D., Noble, J.A., 2016b. Automatic bone segmentation in ultrasound images using local phase features and dynamic programming. International Symposium on Biomedical Imaging (ISBI) , In proceedings.

[7] Jia, R., Mellon, S., Monk, A.P., Murray, D., Noble, J.A., 2015. Three dimensional freehand ultrasound reconstruction using hybrid interpolation. Medical Image Understanding and Analysis , 169–174.

[8] Jia, R., Mellon, S., Monk, A.P., Murray, D., Noble, J.A., 2016c. Globally optimal registration for describing joint kinematics. Procedia of Computer Science, International Conference of Medical Image Understanding and Analysis .

[9] Jia, R., Mellon, S., Monk, P., Murray, D., Noble, J.A., 2016d. A computer-aided tracking and motion analysis with ultrasound (cat & maus) system for the description of hip joint kinematics. International Journal of Computer Assisted Radiology and Surgery 11, 1965–1977.

[10] Masum, M.A., Pickering, M., Lambert, A., Scarvell, J., Smith, P., 2014a. Accuracy assessment of tri-plane b-mode ultrasound for non-invasive 3d kinematic analysis of knee joints. Biomedical Engineering Online 13, 1.

[11] Masum, M.A., Pickering, M., Lambert, A., Scarvell, J., Smith, P., 2014b. knee-deep sensing (feature article). Electronics Letters (The IET) 50.

[12] Monk, A.P., 2011. The patellofemoral joint : form and function. Thesis University of Oxford.

[13] Monk, A.P., Chen, M., Mellon, S., Gibbons, M., Beard, D.J., Murray, D.W., Gill, H.S., 2013. Comparison of in-vivo coronal plane patella tracking following knee arthroplasty using the maus technique. Bone & Joint Journal Orthopaedic Proceedings Supplement 95, 10–10.

[14] Nazarian, L.N., 2008. The top 10 reasons musculoskeletal sonography is an important complementary or alternative technique to mri. American Journal of Roentgenology 190, 1621–1626.

[15] Robertson, G., Caldwell, G., Hamill, J., Kamen, G., Whittlesey, S., 2013. Research methods in biomechanics, 2E. Human Kinetics.

[16] Ross, A., 2004. Procrustes analysis. Course Report, Department of Computer Science and Engineering, University of South Carolina .

[17] Rouhandeh, A., Joslin, C., Qu, Z., Ono, Y., 2014. Quantification of soft tissue artefacts using motion capture data and ultrasound depth measurements. World Academy of Science, Engineering and Technology, International Journal of Medical, Health, Biomedical, Bioengineering and Pharmaceutical Engineering 8, 334–338.

[18] Shellikeri, S., Girard, E., Setser, R., Bao, J., Cahill, A., 2016. Metal artefact reduction algorithm for correction of bone biopsy needle artefact in paediatric c-arm ct images: a qualitative and quantitative assessment. Clinical Radiology .

[19] Souza, R.B., Draper, C.E., Fredericson, M., Powers, C.M., 2010. Femur rotation and patellofemoral joint kinematics: a weight-bearing magnetic resonance imaging analysis. Journal of Orthopaedic & Sports Physical Therapy 40, 277–285.

[20] Stagni, R., Fantozzi, S., Cappello, A., Leardini, A., 2005. Quantification of soft tissue artefact in motion analysis by combining 3d fluoroscopy and stereophotogrammetry: a study on two subjects. Clinical Biomechanics 20, 320–329.

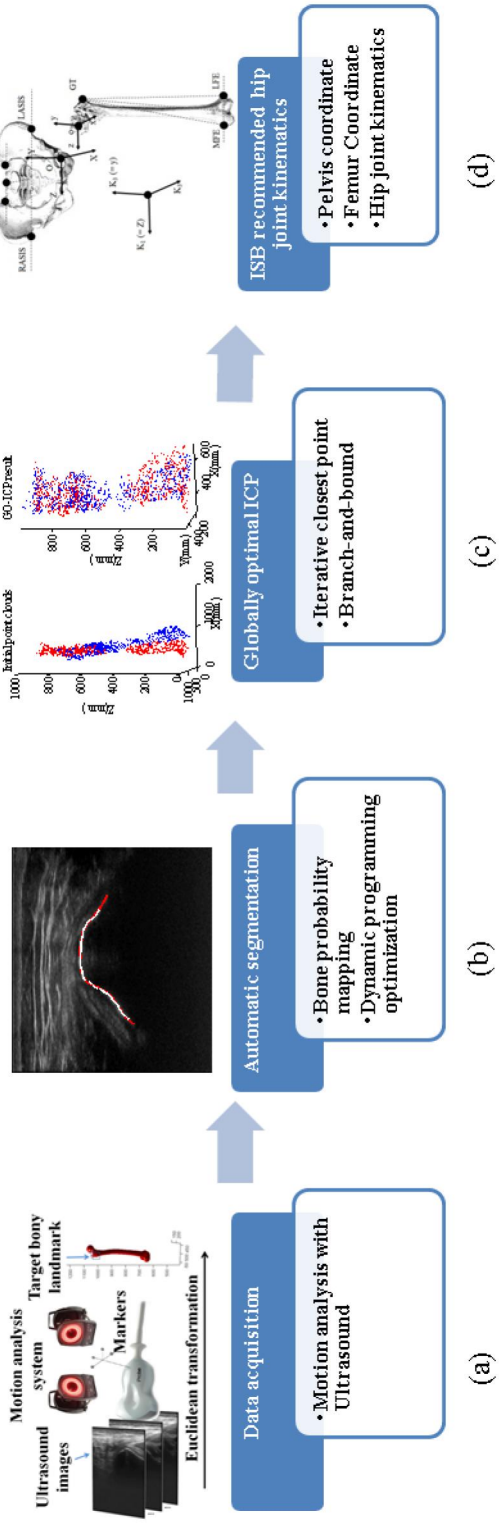

Figure 1: Schematic of the computer-aided tracking and motion analysis with ultrasound (CAT & MAUS) system [9].

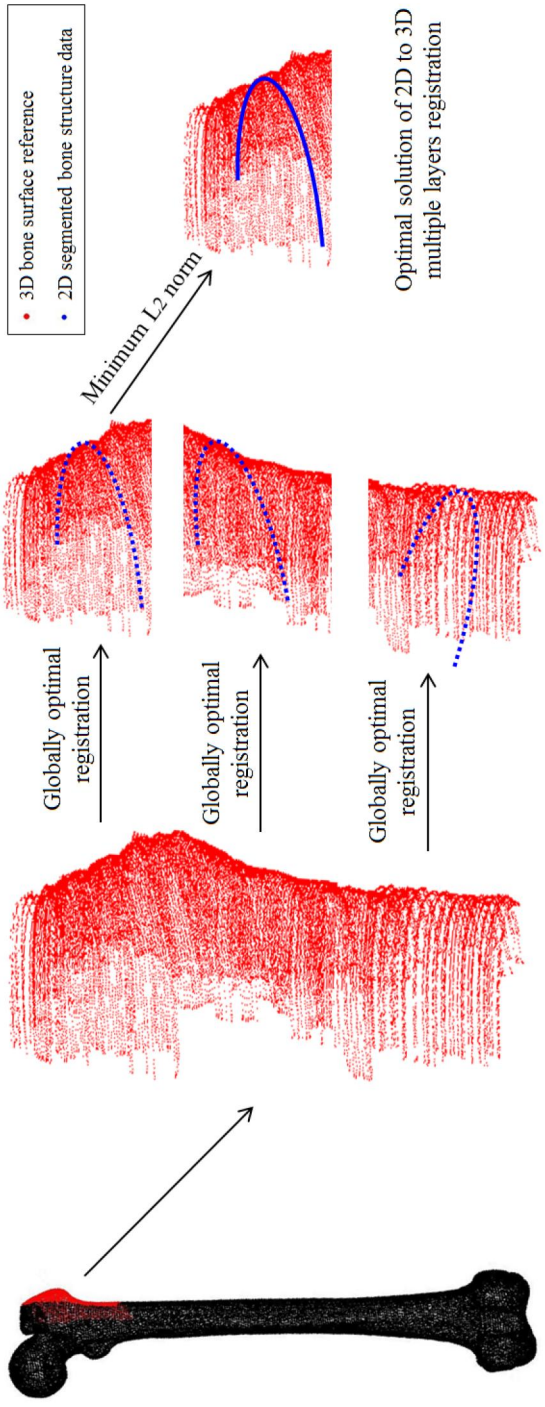

Figure 2: An illustration of multiple segments globally optimal registration.

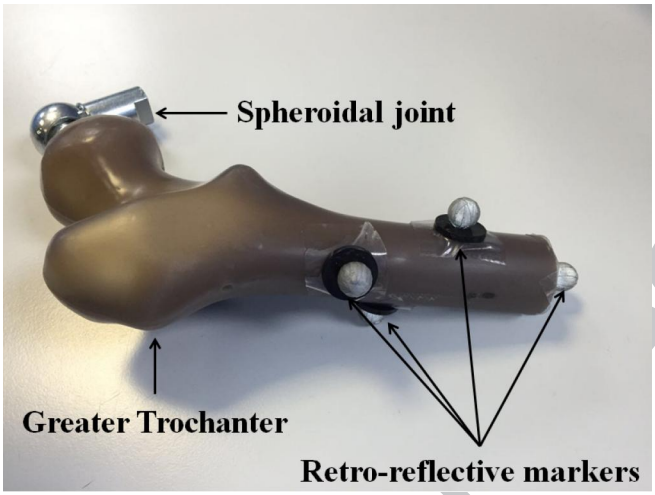

(a)

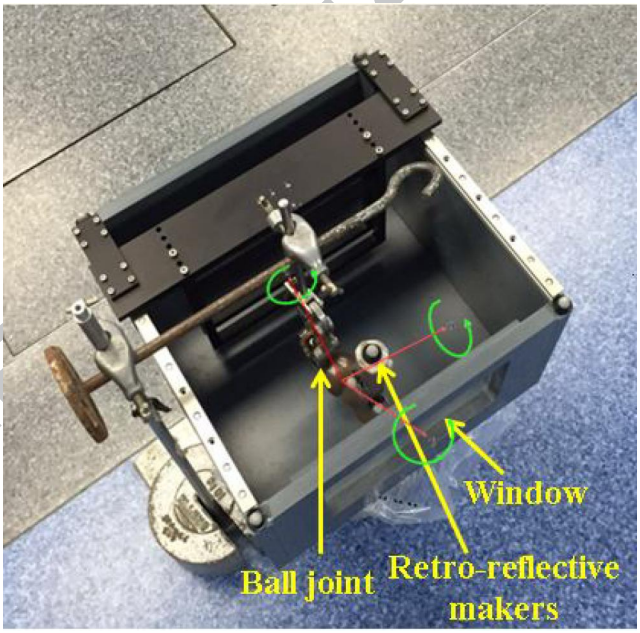

(b)

Figure 3: *In-vitro* experiment, (a) Proximal femur phantom with a socket ball joint, and (b) experiment set up.

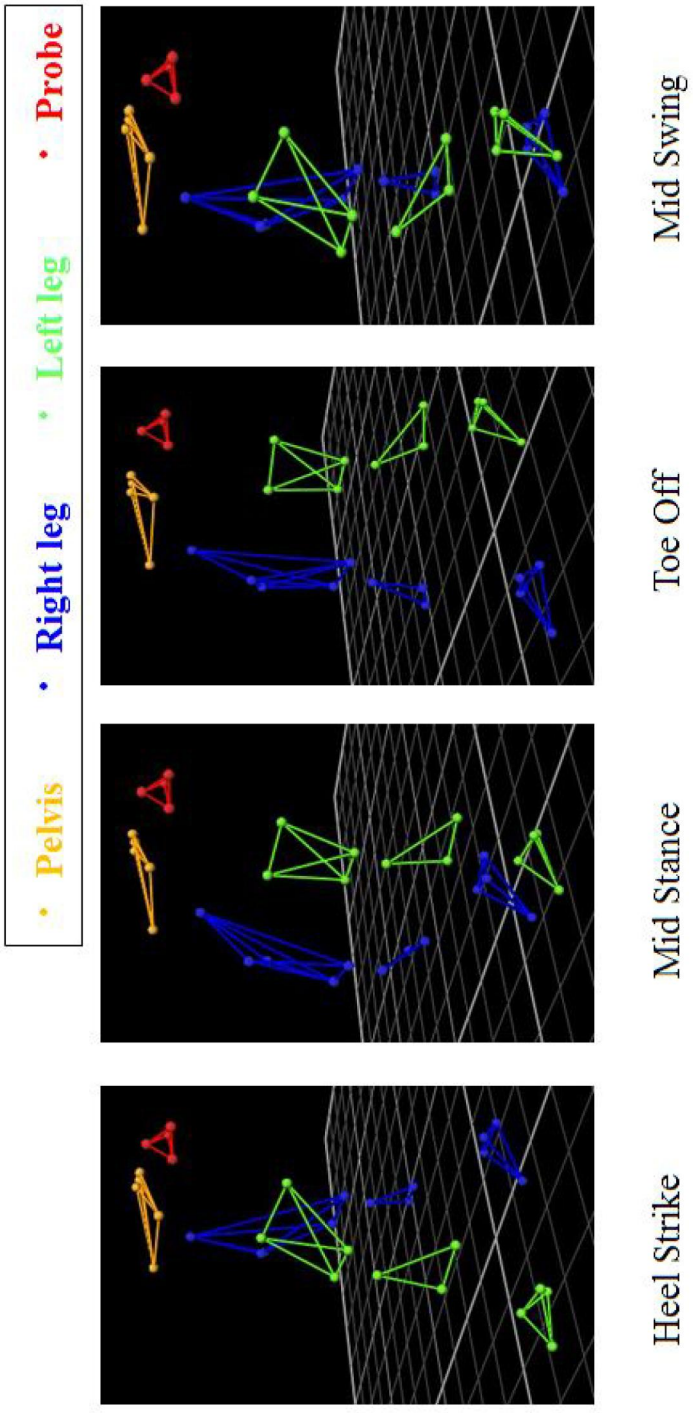

Figure 4: *Four gait poses (heel strike, mid stance, toe off and mid swing).*

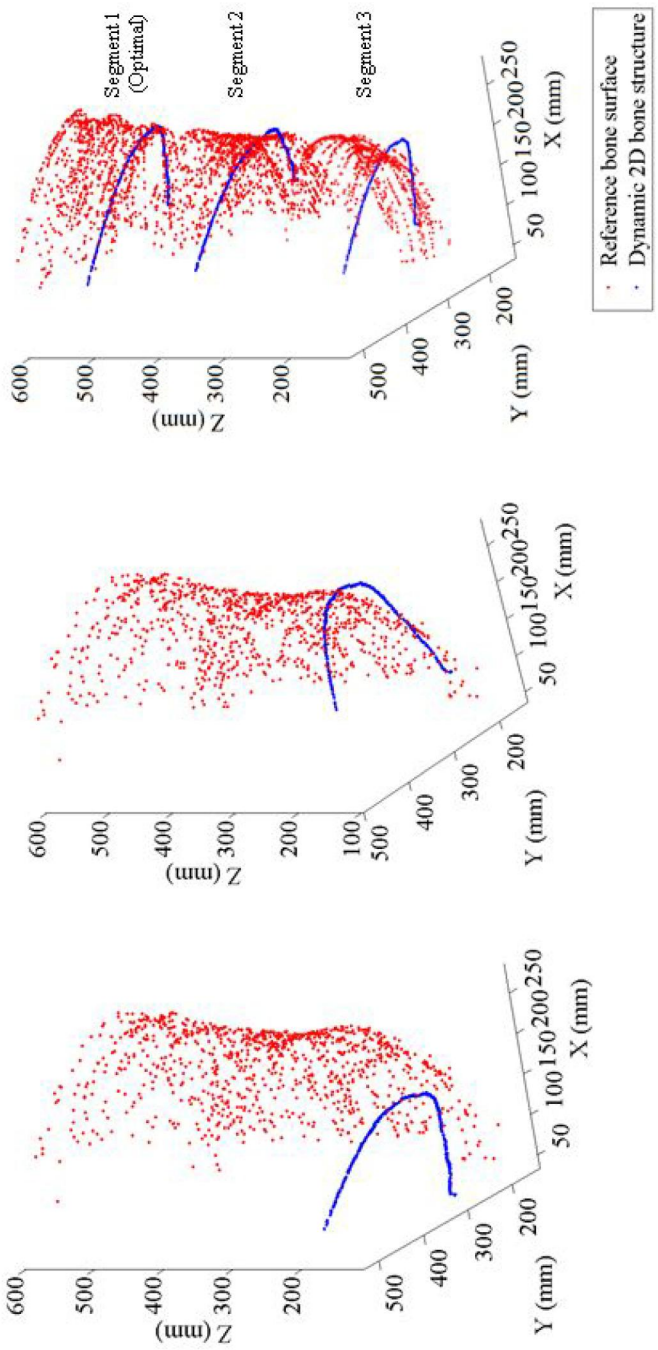

Figure 5: A visual comparison of the registration from the segmented bone contour in 3D space in each of these 20 US frames to the full reference surface and each of three split segments, (a) before registration, (b) after registration to full reference surface, and (c) after registration to multiple segments.

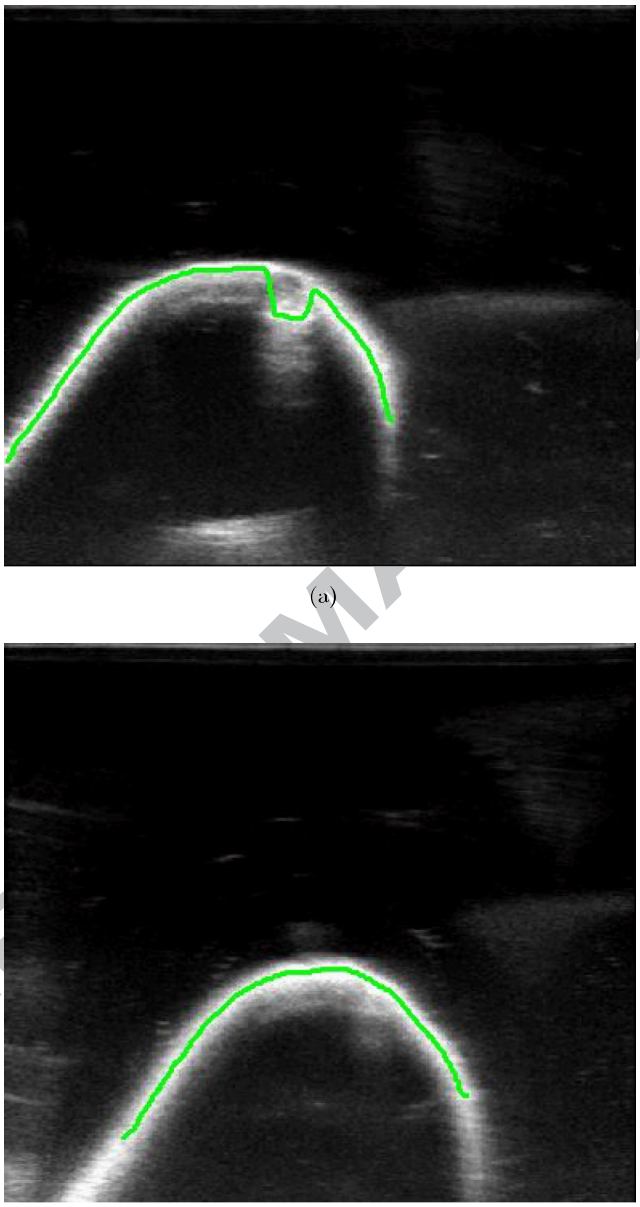

(a)

(b)

Figure 6: Automatically segmented bone structures, (a) a bone structure with a notch, and (b) a plain bone structure.

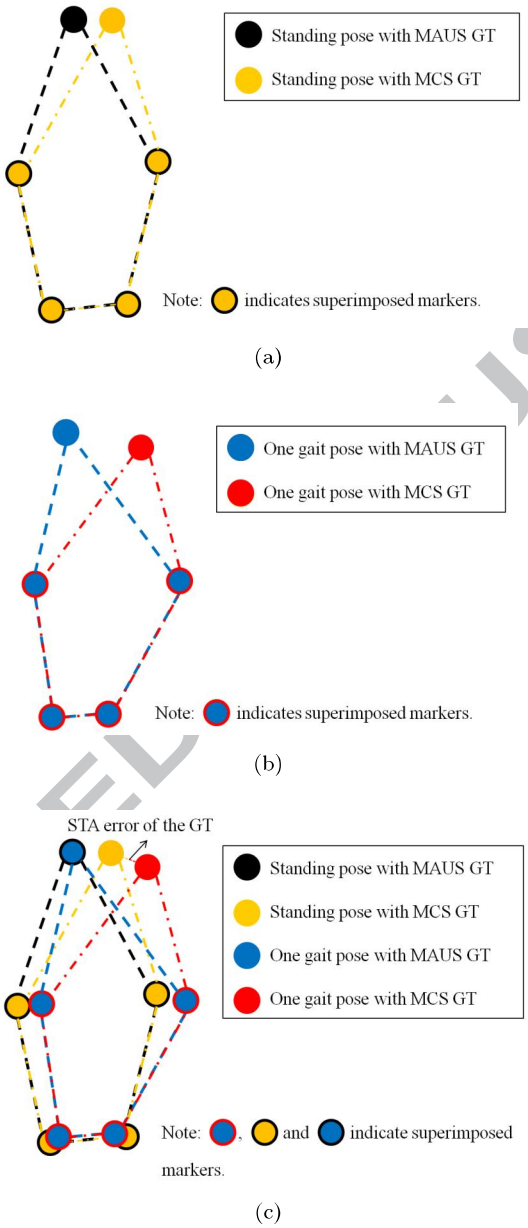

Figure 7: An illustration of the comparison between the femur shapes modelled by each of MCS alone and CAT & MAUS (a) at the standing pose, (b) at one example gait pose, and (c) is the combination of (a) and (b).

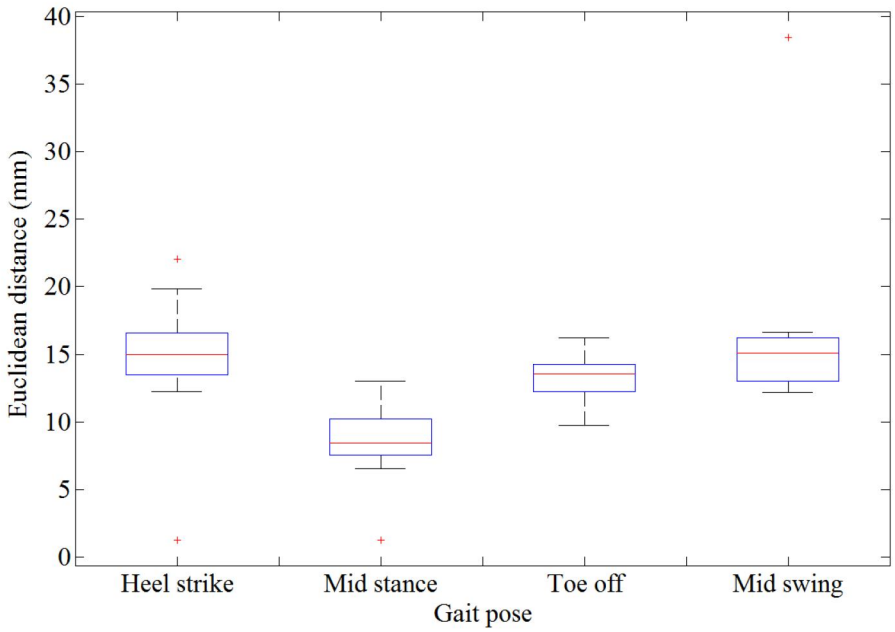

Figure 8: The Euclidean distances between the CAT & MAUS GT and the MCS GT of the superimposed femur shapes at each of four different poses (heel strike, mid stance, toe off and mid swing).

Position	Full Surface	Segment 1	Segment 2	Segment 3	Optimal Reference Index
1	0.0963	**0.0100**	0.0154	0.0372	Segment 1
2	0.0411	**0.0136**	0.0308	0.0613	Segment 1
3	0.0307	0.0094	**0.0075**	0.0147	Segment 2
4	0.0420	0.0154	**0.0120**	0.0217	Segment 2
5	0.0312	0.0212	**0.0146**	0.0238	Segment 2
6	0.0330	**0.0097**	0.0173	0.0261	Segment 1
7	0.0202	**0.0099**	0.0148	0.0230	Segment 1
8	0.0495	0.0092	**0.0091**	0.0248	Segment 2
9	0.0337	0.0205	**0.0118**	0.0333	Segment 2
10	0.0314	0.0214	**0.0109**	0.0114	Segment 2
11	0.0247	0.0211	**0.0173**	0.0726	Segment 2
12	0.0701	**0.0053**	0.0122	0.0600	Segment 1
13	0.0753	0.0197	**0.0113**	0.0427	Segment 2
14	0.0869	**0.0067**	0.0140	0.0536	Segment 1
15	0.0974	**0.0074**	0.0113	0.0338	Segment 1
16	0.0534	**0.0096**	0.0102	0.0180	Segment 1
17	0.0315	**0.0309**	0.0168	0.0417	Segment 2
18	0.0725	**0.0117**	0.0217	0.0430	Segment 1
19	0.0381	0.0159	**0.0101**	0.0144	Segment 2
20	0.0975	0.0117	**0.0107**	0.0508	Segment 2

(a)

Position	Full Surface	Segment 1	Segment 2	Segment 3	Optimal Reference Index
1	−11.30°	−1.67°	−2.62°	−9.13°	Segment 1
2	20.53°	−2.45°	−5.91°	−6.99°	Segment 1
3	−7.02°	−3.91°	2.97°	−3.53°	Segment 2
4	8.97°	−5.51°	1.21°	6.16°	Segment 2
5	−28.11°	−1.15°	5.12°	5.17°	Segment 1
6	−5.75°	−3.43°	16.30°	9.65°	Segment 1
7	−22.72°	−3.33°	13.27°	−6.02°	Segment 1
8	−12.22°	−6.76°	6.61°	−5.61°	Segment 3
9	−28.60°	−17.59°	9.73°	28.44°	Segment 2
10	6.98°	16.91°	0.78°	−5.48°	Segment 2
11	−28.93°	−17.19°	5.72°	7.25°	Segment 2
12	−23.41°	−3.02°	3.05°	−5.55°	Segment 1
13	9.69°	−7.75°	20.49°	−15.99°	Segment 1
14	−5.19°	−4.13°	5.66°	−7.59°	Segment 1
15	−4.77°	−4.02°	4.07°	−5.50°	Segment 1
16	4.60°	−2.83°	9.68°	5.95°	Segment 1
17	−32.27°	−3.13°	19.59°	−9.89°	Segment 1
18	−7.74°	−3.77°	4.47°	−7.87°	Segment 1
19	4.31°	−5.16°	0.71°	5.62°	Segment 2
20	−8.28°	−1.60°	1.55°	−4.57°	Segment 2

(b)

Table 1: Optimal reference index comparison, (a) the normalised L_2 norms of registrations to each of the full reference surface and those three segments, and the reference index with the minimum L_2 norm (the lowest L_2 norms were bold), and (b) the mean rotation angle difference between the MCS ground truth and results from the registrations to each of the full reference surface and those three segments of the femur phantom, and the reference index with the minimum absolute value of the mean rotation angle difference. Mismatched optimal reference indexes compared to (a) are highlighted in gray colour.

Subject	Heel Strike	Mid Stance	Toe off	Mid Swing
1	0.03	0.01	0.01	0.03
2	0.03	0.01	0.02	0.06
3	0.07	0.01	0.01	0.03
4	0.02	0.02	0.02	0.03
5	0.12	0.02	0.02	0.03
6	0.07	0.02	0.03	0.04
7	0.03	0.01	0.02	0.02
8	0.02	0.02	0.02	0.02
9	0.04	0.01	0.02	0.03
10	0.03	0.03	0.03	0.03

(a)

Subject	Heel Strike	Mid Stance	Toe off	Mid Swing
1	0.25	0.22	0.15	0.29
2	0.22	0.24	0.18	0.25
3	0.13	0.05	0.04	0.12
4	0.27	0.15	0.11	0.26
5	0.11	0.21	0.21	0.22
6	0.25	0.14	0.20	0.27
7	0.22	0.10	0.16	0.25
8	0.22	0.08	0.17	0.21
9	0.16	0.19	0.17	0.24
10	0.18	0.20	0.18	0.19

(b)

Table 2: The Procrustes distances between the femur shape at four different poses (heel strike, mid stance, toe off and mid swing) and the reference femur shape at the standing pose, (a) for the CAT & MAUS femur shape, and (b) for the MCS femur shape